Marine and Petroleum Geology xxx (2012) 1–11

Contents lists available at SciVerse ScienceDirect

Marine and Petroleum Geology

journal homepage: www.elsevier.com/locate/marpetgeo

Seismic velocities on the Nova Scotian margin to estimate gas hydrate and free gas concentrations

Angela Schlesinger [a,*], Janette Cullen [b], George Spence [a], Roy Hyndman [c], Keith Louden [d], David Mosher [e]

[a] School of Earth and Ocean Sciences, University of Victoria, Bob Wright Centre, P.O. Box 3065 STN CSC, Victoria, BC V8W 3V6, Canada
[b] Department of Earth Sciences, 1459 Oxford Street, Dalhousie University, NS B3H 4R2, Canada
[c] Pacific Geoscience Centre, Geological Survey of Canada, P.O. 6000, Sidney, BC V8L 4B2, Canada
[d] Department of Oceanography, Dalhouise University, 1355 Oxford Street, Halifax, NS B3H 4R2, Canada
[e] Geological Survey of Canada-Atlantic, Bedford Institute of Oceanography, P.O. Box 1006, Dartmouth, NS B2Y 4A2, Canada

ARTICLE INFO

Article history:
Received 2 September 2011
Received in revised form
6 February 2012
Accepted 20 March 2012
Available online xxx

Keywords:
Ocean-bottom seismometers
Wide-angle reflections
Travel-time tomography
2-D velocity models
Nova Scotia
Gas hydrate concentrations
Free gas concentration
BSR

ABSTRACT

This article provides new constraints on gas hydrate and free gas concentrations in the sediments at the margin off Nova Scotia. Two-dimensional (2-D) velocity models were constructed through simultaneous travel-time inversion of ocean-bottom seismometer (OBS) data and 2-D single-channel seismic (SCS) data acquired in two surveys, in 2004 and 2006. The surveys, separated by ~5 km, were carried out in regions where the bottom-simulating reflection (BSR) was identified in seismic reflection datasets from earlier studies and address the question of whether the BSR is a good indicator of significant gas hydrate on the Scotian margin. For both datasets, velocity increases by 200–300 m/s at a depth of approximately 220 m below seafloor (mbsf), but the results of the 2006 survey show a smaller velocity decrease (50–80 m/s) at the base of this high-velocity layer (310–330 mbsf) than the results of the 2004 survey (130 m/s). When converted to gas hydrate concentrations using effective medium theory, the 2-D velocity models for both datasets show a gas hydrate layer of ~100 m thickness above the identified BSR. Gas hydrate concentrations are estimated at approximately 2–10% for the 2006 data and 8–18% for the 2004 survey. The reduction in gas hydrate concentration relative to the distance from the Mohican Channel structure is most likely related to the low porosity within the mud-dominant sediment at the depth of the BSR. Free gas concentrations were calculated to be 1–2% of the sediment pore space for both datasets.

1. Introduction

Gas hydrates contain significant amounts of hydrocarbon gas, and so the identification and mapping of gas hydrate occurrences are important to define a potential massive energy resource. Bottom-simulating reflections (BSR's), first identified in seismic reflection data at the Blake Ridge (Tucholke et al., 1977), have been used as an indirect indicator for the presence of gas hydrate and underlying free gas. Ruppel et al. (2011) conclude that the presence of a BSR usually indicates that some gas hydrate, most commonly at low saturation, occurs near the base of the gas hydrate stability zone (GHSZ). BSRs are common in the accretionary sedimentary prisms of active margins but are less common for passive margins. An important question is whether this difference represents much less hydrate on passive margins or only less prominent BSRs.

A few areas may host gas hydrate without a visible BSR, such as portions of the Blake Ridge (Holbrook et al., 1996) and the Gulf of Mexico (Dai et al., 2004; GOM 2009). Studies by Xu and Ruppel (1999) show that a missing BSR in a gas hydrate-prone area might be due to low methane flux into GHSZ. Other possibilities include local perturbations in temperature, salinity and/or methane flux (Ruppel et al., 2011). However, Haacke et al. (2007) argue that passive margins without an observable BSR are unlikely to contain significant quantities of gas hydrate. We therefore have focused on areas with a clear BSR with some data extending to where the BSR is not clear.

The passive margin off eastern Canada was widely mapped during the past 40 years by the hydrocarbon exploration industry. In 1998/9 the Geological Survey of Canada (GSC) collected a total of 34,000 km of two-dimensional (2-D) multi-channel seismic (MCS) data on the Scotian Slope. Therefore, an extensive database of seismic reflection lines exists for the east coast of Canada. The data were recently used by Mosher (2011) to estimate the distribution of gas hydrate based on the area where a BSR can be identified

* Corresponding author. Tel.: +1 250 721 6188; fax: +1 250 721 6200.
E-mail address: schlesin.angela@googlemail.com (A. Schlesinger).

0264-8172/$ – see front matter © 2012 Elsevier Ltd. All rights reserved.
doi:10.1016/j.marpetgeo.2012.03.008

confidently. However, estimates of gas hydrate concentration are poorly constrained – no gas hydrate has been recovered on the Canadian Atlantic margin, and there has been limited interpretation of hydrate occurrence based on geophysical downhole logs (Thurber Consultants Ltd.; Neave, 1990) that has not been confirmed or calibrated by analysis of recovered hydrate.

Important constraints on gas hydrate concentrations are derived from seismic velocities determined from recordings of wide-angle reflections and refractions on ocean-bottom seismometers (OBS) and long-offset MCS streamer systems. Recent one-dimensional (1-D) velocity-depth profiles were obtained from waveform tomography on a 45 km long MCS profile (Delescluse et al., 2011). Mosher (2011) reported velocity results from four OBS surveys on the Atlantic margin, based on 1-D interpretations of individual OBSs. However, in only one survey (LeBlanc et al., 2007) were seismic velocities converted to gas hydrate and free gas concentrations, using an effective medium model (Dvorkin et al., 1999) to obtain estimates of 2–6% bulk gas hydrate and less than 1% free gas in the pore space.

In this paper, we provide improved constraints on gas hydrate and free gas concentrations and volumes on the Atlantic margin of Canada, through careful determination of seismic velocities in the region of the Mohican Channel (Fig. 1) where a prominent BSR was identified. For two surveys, in 2004 and 2006, we constructed 2-D models of velocity through simultaneous inversion of travel-times from arrays of OBSs and from 2-D single-channel seismic (SCS) profiles.

2. Seismic data acquisition and processing

2.1. Ocean-bottom seismometer and single-channel seismic data

In July 2004, an OBS array of nine instruments was deployed on the Scotian slope in approximately 1550 m water depth in the vicinity of the Mohican Channel (Fig. 1), in a region where the BSR was identified in 2-D MCS reflection data (Mosher et al., 2004). Additional 2-D single-channel seismic reflection (SCS) data and high resolution Huntec DTS sparker data were acquired in the same survey to provide information about the shallow seismic stratigraphy (Mosher, 2004). The research vessel CCGS Hudson towed an array of two generator–injector (GI)-guns (Seismic System Inc.; 1.7 L generator volume; 1.7 L injector volume) at a depth of approximately 2 m. The shots were fired by distance at an interval of 20 m; the average ship speed was 4.5 knots. The OBS instruments were aligned in a 2-D profile with a horizontal separation of approximately 100 m. Shots were fired to offsets of 4.5 km to the south and 6. 3 km to the north. A SCS reflection line was collected simultaneously for a total length of ~12 km (Fig. 1).

In August 2006, a second OBS survey was carried out in an area ~5 km south of the 2004 survey on the Scotian Slope in the vicinity of the Mohican Channel. A total of 19 instruments were deployed in two independent arrays in an approximate water depth of 1650 m, with nine stations in a western profile and ten stations in an eastern profile. The arrays extended from an area in the west, near the south-eastern sidewall of the Mohican Channel where the BSR was identified in the 2-D MCS reflection data (Cullen et al., 2008), to an adjacent area in the east where no BSR is apparent. Within this survey the same OBS instruments and GI-gun array as for the 2004 survey were used. However, the shot interval was 15 m and the spatial OBS separation averaged 900 m. The length of the shot line and the coincident 2-D SCS reflection line above the western OBS array was 12 km from west to east. The shot line was repeated for the eastern OBS array. However, only the data from the western OBS array were analysed in this paper.

The OBS data of both surveys (2004 and 2006) were sampled at an interval of 1 ms up to 200 Hz with a dominant frequency of 45 Hz. However, prominent low-frequency noise of unknown origin was present at 8 Hz in both datasets. Thus, a simple bandpass filter from 10 to 200 Hz was applied to improve the data quality.

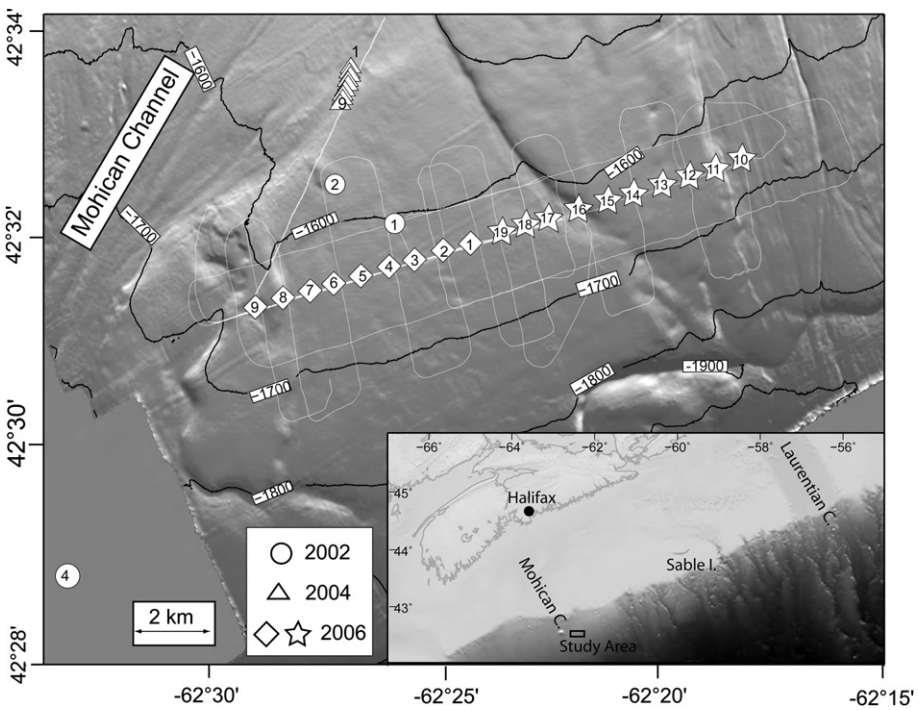

Figure 1. Location of the study area (box within the smaller map) on the Scotian margin in the vicinity of the Mohican Channel. The three different deployments from 2002 (circles), 2004 (triangles), and 2006 (diamonds and stars) are shown. The 2-D single-channel seismic (SCS) data and OBS data from 2004 and 2006 (diamonds only) are modelled and discussed in this paper.

Please cite this article in press as: Schlesinger, A., et al., Seismic velocities on the Nova Scotian margin to estimate gas hydrate and free gas concentrations, Marine and Petroleum Geology (2012), doi:10.1016/j.marpetgeo.2012.03.008

2.2. Relocation of the OBS instruments

The OBS positions, clock drifts and the shot locations need to be known precisely in order to get a good velocity model. Although the OBS deployment and retrieval positions could be determined accurately with the ship's Global Positioning System (GPS), the instruments could drift by several hundred metres from the point of deployment while sinking to the seafloor. Therefore, the actual seafloor position of an instrument depends on the local water depth and the current speed. Since the internal clocks also drift, an approximate clock drift measurement is made when the OBS is recovered by comparing the OBS clock time to an accurate satellite time. The shot positions recorded from the ship also have an uncertainty of the order of tens of metres (e.g. Zykov, 2006).

The OBS and shot relocation is an inverse problem in which the objective is to find the seafloor location of the OBS, the shot positions, and a time correction that minimizes the error between the observed and calculated travel-times of the seismic signal through the water column. For this study the source-receiver localization (SRL) scheme of Zykov (2006) was used. It provides a solution for the shot and receiver positions and solves for the GPS clock drift. The SRL is ill-conditioned, because of the small area where the OBS instruments are located in comparison to the shot geometry (Zykov, 2006). The azimuths from far offset shots to the OBSs are concentrated in a narrow region and this causes instability in the solution. Thus, the method uses a regularized inversion approach, by incorporating *a priori* estimates of shot and receiver positions and their uncertainties into the solution (Zykov, 2006).

Direct arrival seismic travel-times were used for the source-receiver localization for both OBS arrays (2004 and 2006). After four iterations, the root-mean-square (RMS) travel-time residual misfit for the 2004 OBS instruments was between 2 and 4 ms, close to the sampling interval. Misfit results for the 2006 OBS instruments were generally less than 2 ms, comparable to the direct arrival travel-time picking uncertainties. The average horizontal drifts during the instrument drop to the seafloor were between 50 and 100 m to the south for the 2004 OBS stations, and 100–200 m to the west for the 2006 OBSs.

3. Data characteristics

3.1. Seismic reflection data

Within the 2004 2-D SCS reflection and OBS data, reflected arrivals were identified to 800 ms below the seafloor/direct arrival. The subseafloor structure is fairly uniform with reflections that are mostly continuous across the section. A strong amplitude reflection identified on the 2-D SCS reflection data, at ~370 ms below the seafloor (bsf) (Fig. 2a), is recognized as the BSR, consistent with the conclusions of Mosher et al. (2004). However, the expected phase reversal of the BSR, relative to the seafloor reflection, is difficult to identify.

The 2006 2-D SCS reflection data (Fig. 2b) shows a similar set of main reflections as the 2004 2-D SCS reflection data, including the BSR at ~370 ms below the seafloor reflection. The phase of the BSR is still ambiguous in the 2006 2-D SCS reflection data, but at some locations a phase reversal can be tentatively identified.

A 3-D multi-channel seismic dataset acquired and processed by EnCana Ltd. (not shown in this paper) was examined to confirm that the most significant reflections in the 2-D SCS datasets were also identified in the MCS data (Cullen et al., 2008).

3.2. OBS wide-angle reflections and refractions

On some of the 2004 OBS data, refracted arrivals emerging from the direct arrivals were identified over the offset range from approximately 4.5 km–5.1 km (Fig. 3a). In the 2006 OBS data, two first-arrival refracted phases were identified. On almost all OBS instruments, one phase extended over an offset range from ~4 km to nearly 6 km (Fig. 3b); a second phase, identified on only four OBSs, extended an additional distance of ~750 m (Fig. 3b), and its amplitude decreased with distance. Despite the long shot profiles in both surveys (2004 – 12 km, 2006 – 10.5 km), shot-receiver offsets were still not long enough to record refracted arrivals from deeper horizons.

For both the 2004 and 2006 OBS data, near-offset reflections were compared to reflections selected in the 2-D SCS data, to identify the most prominent reflections that are consistent between the two datasets (Fig. 3). The reflected arrivals typically converged and emerged from the direct arrival at an offset of ~4 km, arriving shortly after the first-arrival refractions. Most reflections could be picked confidently only for offsets less than ~3 km.

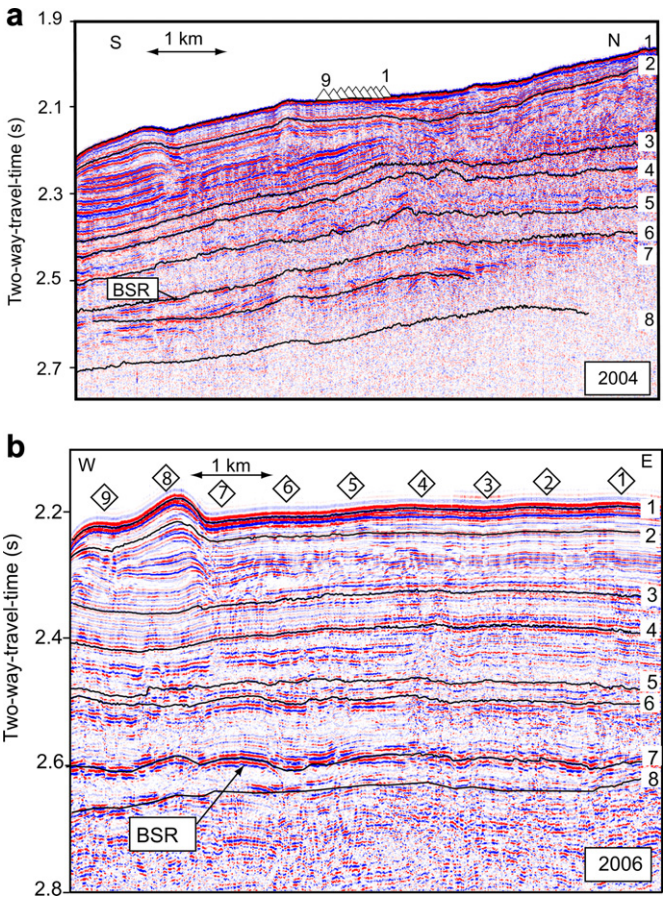

Figure 2. (a) 2-D SCS reflection profile (2004) shows the positions of the nine OBS stations (triangles) with ~100 m instrument separation. Travel-times for the eight identified reflections were inverted simultaneously with travel-times for reflections and refractions from the OBSs. The BSR (reflection 6) was identified at approximately 350 ms two-way-travel-time (TWT) below the seafloor. (b) 2-D SCS reflection profile (2006) shows the positions of the nine OBS stations (diamonds) used in this study with an instrument separation of approximately 900 m. The eight identified horizons on the 2-D SCS profile were used for the seismic travel-time tomography simultaneously with the travel-times for reflections and refractions from the nine OBSs. The BSR (reflection 7) is identified at approximately 350 ms TWT below the seafloor.

4. Modelling of refraction and reflection travel-times for P-wave velocities

We utilized the seismic travel-time inversion algorithm of Zelt and Smith (1992), which has been widely applied in gas hydrate-

Please cite this article in press as: Schlesinger, A., et al., Seismic velocities on the Nova Scotian margin to estimate gas hydrate and free gas concentrations, Marine and Petroleum Geology (2012), doi:10.1016/j.marpetgeo.2012.03.008

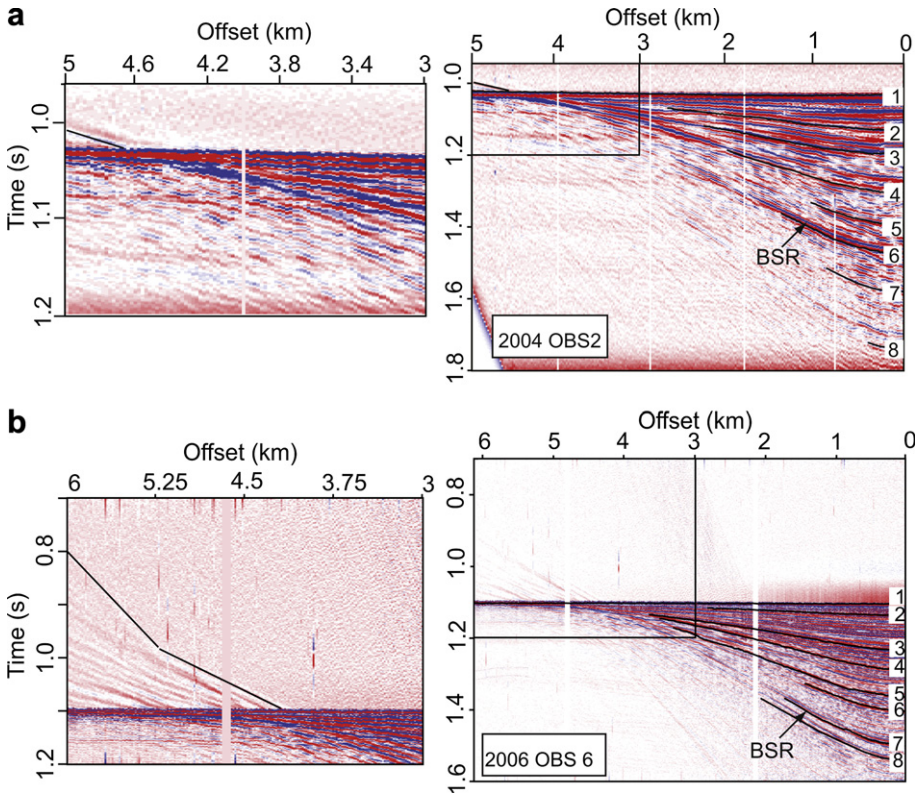

Figure 3. (a) Example of the 2004 data (OBS 2) with a hyperbolic move-out correction to flatten the seafloor using 1480 m/s. The first-arrival refraction (enhanced box – left) and the eight main reflections including the BSR were used for the seismic travel-time tomography in the 1-D and 2-D modelling schemes. (b) Example the 2006 data (OBS 6) with a hyperbolic move-out correction to flatten the seafloor using 1480 m/s. The first-arrival refractions (enhanced box – left) and the eight main reflections including the BSR were used for the seismic travel-time inversion. The second refraction was only identified on four OBSs and was not further used for the seismic travel-time modelling. (Solid lines for both datasets show the picked reflected and refracted arrivals.)

related studies (e.g. LeBlanc et al., 2007; Jaiswal et al., 2006; Lopez et al., 2010; Chabert et al., 2011). The algorithm uses ray-tracing for forward modelling followed by damped-least-squares inversion. Within the inversion step, the model parameters (velocity and depth) are modified to minimize the difference (misfit) between the observed and the predicted travel-times.

To obtain an appropriate starting model for the 2-D travel-time inversion using all nine OBSs in the 2004 survey, 1-D velocity profiles were obtained for each OBS individually (Fig. 4). Starting with the water layer, layer-stripping was used in which the top layer was modelled first and then held fixed. Forward modelling and inversion were iteratively repeated until the solution converged with a χ^2 value less than or equal to 1, i.e., the root-mean-square (RMS) travel-time misfit fell to 10 ms which is comparable to the pick uncertainty.

The 1-D vertical profiles were used to form a starting model for a 2-D analysis. Seismic travel-times from the SCS vertical incidence reflections and from wide-angle reflections and refractions identified on the OBS data were all modelled simultaneously, using the tomographic inversion scheme of Zelt and Smith (1992). The wide-angle reflections and refractions control the velocities of the model, while reflections from the vertical incidence data provide additional control on the interface depths and detailed subsurface structure.

Similar to the 2004 data analysis, wide-angle reflections and refractions of the OBS data from the 2006 survey were modelled simultaneously with the SCS travel-time data.

The ray-coverage for the shallower layers (<100 mbsf) is much sparser for the 2006 data (Fig. 5), which means that the shallow velocities are essentially 1-D profiles. This is because the instrument spacing was much wider in 2006 than in 2004 (900 m vs 100 m). The actual length of the profile that could be modelled with the 2006 data is also much greater than the 2004 modelled profile (8 km vs 2 km). Since the ray-coverage and path lengths over which velocities are calculated increase with depth, the constraints on average velocity for the deeper region are also improved.

The final 2-D velocity model based on the OBS and SCS data is shown in Figure 6 for the 2004 survey and in Figure 7 for the 2006 survey. The velocity contrast modelled with the 2004 OBS data appears to be larger than that modelled with the 2006 data, even though the ray-coverage is highest for the deeper layers (layer 7 – Fig. 5). The velocity contrasts likely represent real structural differences between the two regions that are only ~5 km apart.

5. Results

5.1. 2004 OBS data: 1-D velocity models

Since the seismic reflection data show that the sediment structure is relatively uniform laterally with near-horizontal layering, the 1-D velocity models for the nine OBSs of the 2004 survey provide meaningful information on the vertical velocity structure. However, all 1-D models are independent and treat noise and local structure complexity individually. The velocity profiles show a velocity increase of 210–450 m/s at a depth of 200–250 mbsf at most locations, with the exception of OBSs 4 and 5 which have smaller velocity contrasts (Fig. 4), probably related to the local structure underneath. Velocity decreases by about the same amount at depths of 310–360 mbsf (corresponding to reflection 6 – Figs. 2 and 6) at the expected depth of the BSR

Please cite this article in press as: Schlesinger, A., et al., Seismic velocities on the Nova Scotian margin to estimate gas hydrate and free gas concentrations, Marine and Petroleum Geology (2012), doi:10.1016/j.marpetgeo.2012.03.008

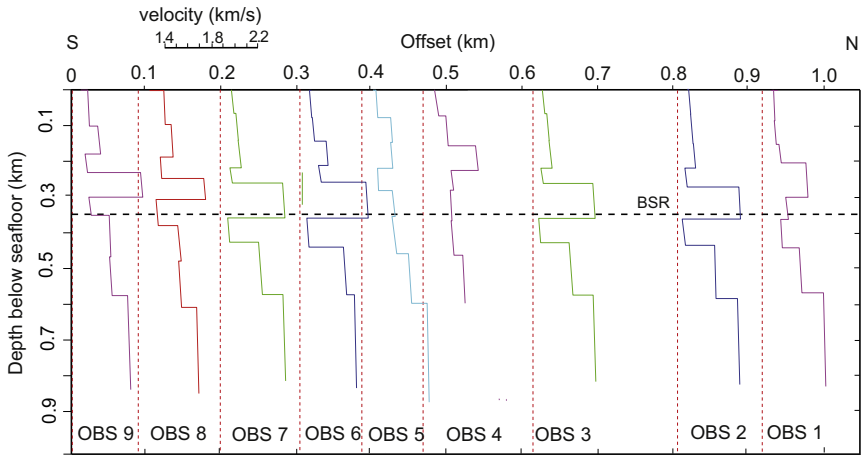

Figure 4. The 1-D velocity-depth models for the nine OBSs from 2004 are shown, where the red dashed lines are positioned at the spatial distances along the OBS line, and represent the origin (1400 m/s) of each velocity profile. The black dashed line indicates the depth of the expected BSR from the 2-D reflection data (Fig. 2a). The velocity increase of 210–450 m/s at ~200–250 mbsf was modelled on all stations except OBSs 4 and 5, where a smaller velocity contrast occurs (see text for details). (For interpretation of the references to colour in this figure legend, the reader is referred to the web version of this article.)

(Fig. 4 – dashed line). At greater depths, modelled velocities generally increase uniformly.

5.2. 2004 OBS and SCS data : 2-D models

Wide-angle reflection and refraction travel-times from all nine OBS stations of the 2004 data, plus travel-times from the 2-D SCS reflection data, were modelled simultaneously to create a 2-D velocity model (Fig. 6). In comparison to the 1-D profiles, the 2-D velocity structure has less variability along the profile. As well, rays travelling from the shots to the receivers constrain the velocity structure over a total profile length of ~2.5 km, much wider than the 900 m length of the OBS array where the 1-D velocity profiles are located. The 2-D velocity model is smoothed over a range of 200–400 m; therefore, locally occurring, complex structures and noise are smoothed as well.

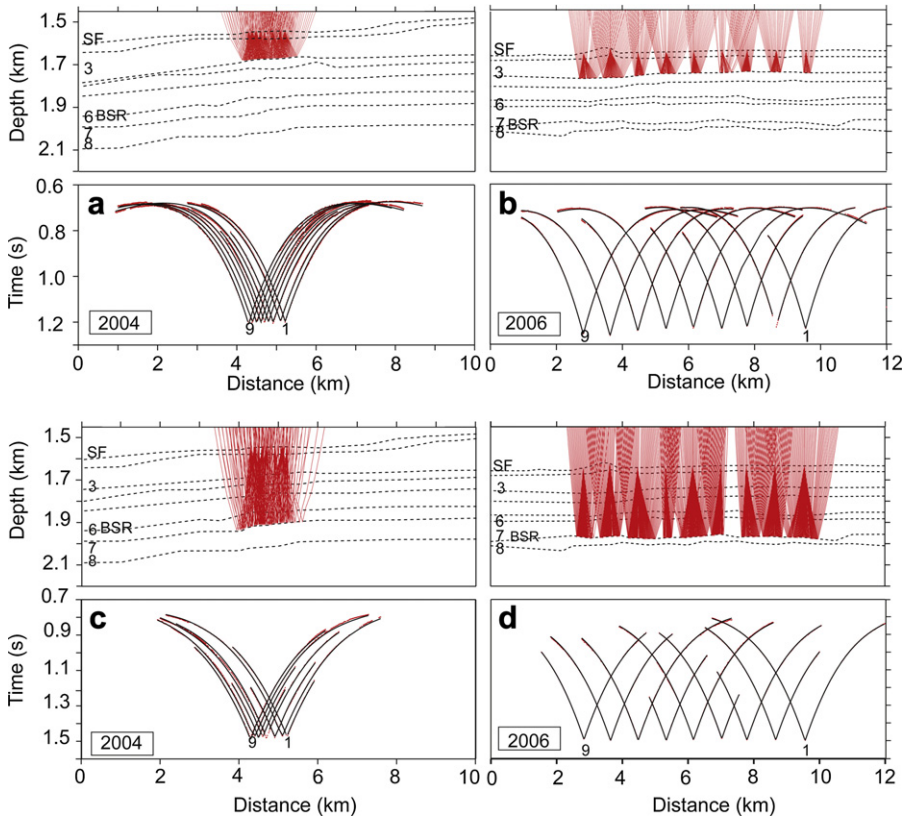

Figure 5. Comparison of ray-tracing and travel-time inversion models for reflections from interface 3 at a depth of approximately 150 mbsf for the 2004 data (a) and 2006 data (b). Ray-coverage for the 2006 OBS data is sparser than for the 2004 data due to the acquisition geometry. Plots show seismic travel-time inversion results (model – black dots) versus seismic travel-time picks (data – red bars) of the OBSs. Both modelled and original data are displayed with a reduced velocity of 1820 m/s. Reflections from interface 7 are shown for the 2004 data (c) and 2006 data (d). Plots show seismic travel-time inversion results (model – black dots) versus the seismic travel-time picks (data – red bars). Both modelled and original data are displayed with a reduced velocity of 1820 m/s. (For interpretation of the references to colour in this figure legend, the reader is referred to the web version of this article.)

Please cite this article in press as: Schlesinger, A., et al., Seismic velocities on the Nova Scotian margin to estimate gas hydrate and free gas concentrations, Marine and Petroleum Geology (2012), doi:10.1016/j.marpetgeo.2012.03.008

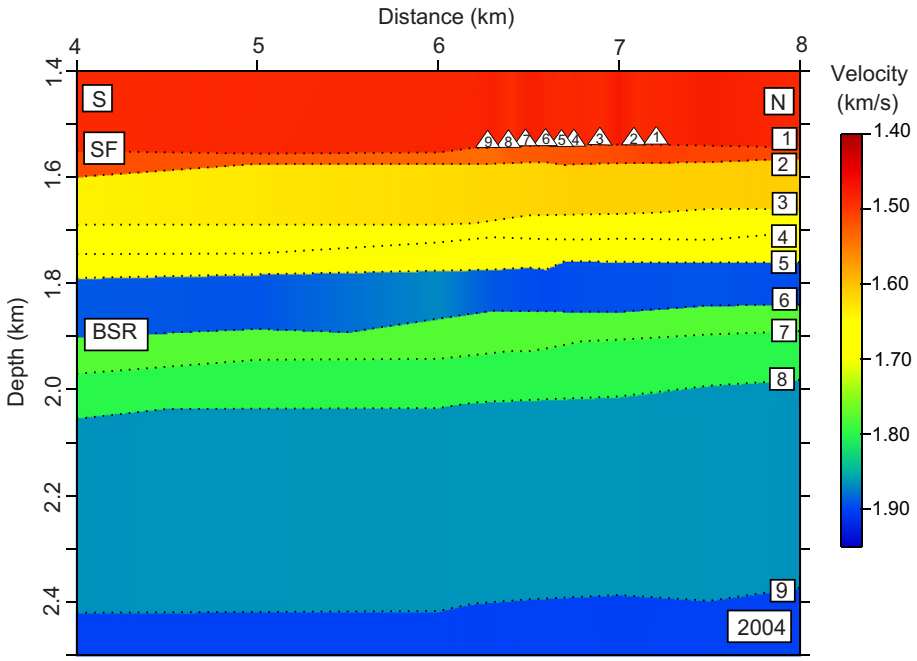

Figure 6. 2004 2-D velocity model from travel-time tomography using arrivals from the nine OBS stations (triangles) and the corresponding 2-D SCS vertical incidence profile (Fig. 2a). The BSR marks the transition to a layer of reduced velocity (1590 m/s) below a high-velocity zone (average 1900 m/s). The numbers indicate the eight main reflections that were used in the travel-time inversion modelling. The velocity model shows a 4 km long section of the whole 12 km long profile that indicates the region of full ray-coverage where the travel-time arrivals provide control on velocities.

In the 2-D velocity model shown in Figure 6, the most prominent feature is a high-velocity layer between interfaces 5 and 6, with a thickness of ~110 m and an average velocity of 1900 m/s. Refractions produced at the top of this layer are observed on almost all OBSs. The velocity of the layer is significantly higher than the average velocity (1600 m/s) between the seafloor and the top of this layer (~220 mbsf). The base of this high-velocity layer, at 310–320 mbsf, corresponds to the BSR identified on the SCS reflections sections (Fig. 2a – reflection 6) and the 2-D MSC reflection data (Mosher et al., 2004).

Below interface 6, a velocity decrease of ~130 m/s was modelled for a layer that has almost the same thickness as the layer above (~100 m) (Fig. 6). The results are similar to those obtained from the 1-D velocity models (Fig. 4), except that the 1-D velocities

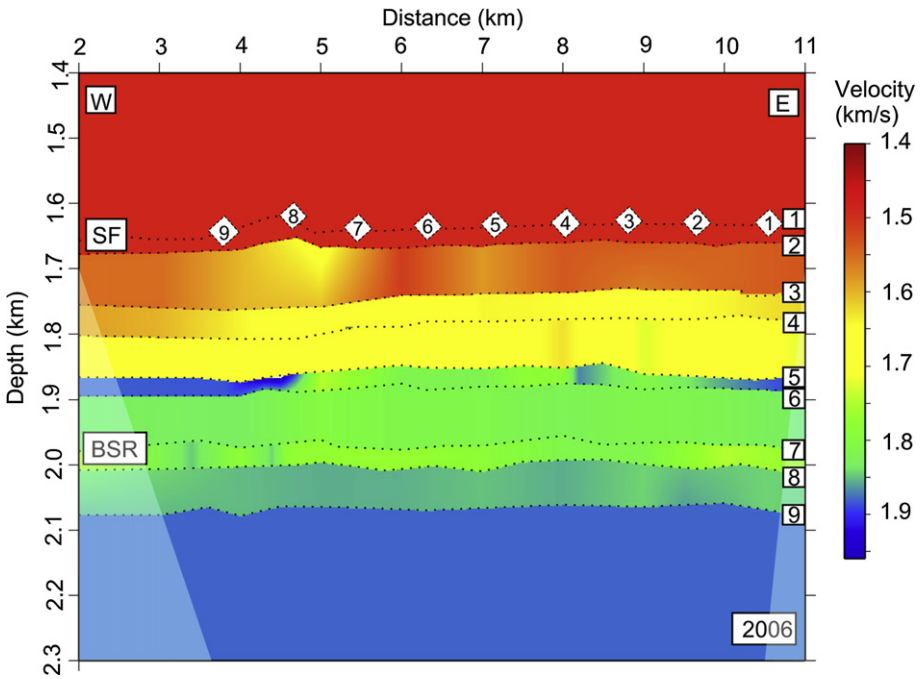

Figure 7. 2006 2-D velocity model from travel-time tomography using arrivals from the nine OBS stations (diamonds) of 2006 and the corresponding 2-D SCS vertical incidence profile. The travel-time inversion results show a small velocity contrast at the BSR depth. Refractions are produced below interface 5 at 210–220 mbsf, where the velocity increases by 200 m/s. The unshaded area indicates the region of ray-coverage, where the travel-time arrivals provide control on velocities. (For interpretation of the references to colour in this figure legend, the reader is referred to the web version of this article.)

Please cite this article in press as: Schlesinger, A., et al., Seismic velocities on the Nova Scotian margin to estimate gas hydrate and free gas concentrations, Marine and Petroleum Geology (2012), doi:10.1016/j.marpetgeo.2012.03.008

are less consistent laterally since each OBS was modelled independently. The velocity contrast at the BSR depth, achieved in the 1-D velocity models, is larger (~300 m/s) than the contrast modelled in the 2-D approach with the same data (~130 m/s).

Below interface 7, the velocity slowly increases to 1800 m/s for layer 8 at a depth of 400 mbsf. With deep reflections on some of the OBSs, layer 9 was modelled with a velocity of 1900 m/s and a base at ~850 mbsf. No vertical incidence data are available to provide additional constraints on the depth of this layer.

5.3. 2006 OBS and SCS data: 2D models

The final 2-D velocity model of the 2006 data simultaneously incorporated seismic travel-time arrivals from the nine OBSs and the 2-D SCS vertical incidence profile (Fig. 7). The velocity increases gradually, from 1490 m/s near the seafloor to 1650 m/s at ~210 mbsf. At that depth, the modelled rays refract at the top of a layer in which the velocity increases sharply to 1820 m/s in the central part of the profile, with indications of higher velocities (>1900 m/s) at the western and eastern ends. This layer has a thickness of only 30–40 m, so its velocity is poorly constrained. However, beneath that interval a thicker (100 m) layer was modelled with similar velocities (1810–1840 m/s), so the transition to higher velocities over this depth range is well-established. The high-velocity layer extends downward to interface 7 at a depth of ~330 mbsf, corresponding to the BSR as identified in the 2-D SCS and 2-D MCS sections (Mosher et al., 2004) (Fig. 2b). Below interface 7, the velocity model shows a small velocity decrease of 50–70 m/s that contrasts with the larger velocity decrease modelled in the 2004 data.

5.4. Sensitivity analysis for layers above and below BSRs

An analysis of sensitivity of the results to perturbations in selected velocity model parameters was performed for the 2004 and 2006 data using the method of Katzman et al. (1994). LeBlanc et al. (2007) used the same method to constrain their error estimates. Velocities are perturbed for a single layer of the final model and then they are held fixed while inverting for the corresponding depth values. The perturbations are made larger until the travel-time residual values increase significantly above the value of the starting model.

For the higher velocity zone above the BSR (Fig. 8a), sensitivity results show that velocities can vary by ±3–5% (±60–100 m/s) for the 2004, but only ±3% (±60 m/s) for the 2006 data. For the low-velocity region below the BSR, the results (Fig. 8b) show that velocities may vary by up to ±3–6% (±50–100 m/s) for the 2006 model, but only up to ±3% (±50 m/s) in the 2004 model.

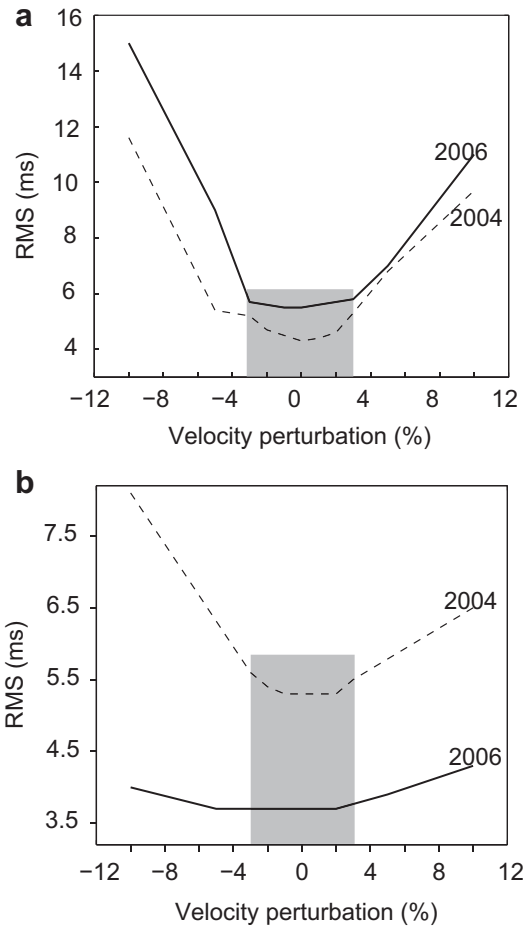

Figure 8. (a) Results of the sensitivity analysis of the 2004 (dashed line) and 2006 (solid line) OBS data for the velocity perturbation of the high-velocity layer above the identified BSR. An approximate estimate of the confidence range for both OBS datasets is indicated by the shaded box. (b) Results of the sensitivity analysis of the 2004 (dashed line) and 2006 (solid line) OBS data for the velocity perturbation of the low-velocity layer below the identified BSR depth. Allowed velocity perturbations are ±3% for the 2004 data (shaded box), but much greater (>±5%) for the 2006 data.

6. Discussion

6.1. Identification of reflected and refracted arrivals

The most significant reflected arrival is identified at the top of the high-velocity region, where the first-arrival refracted waves

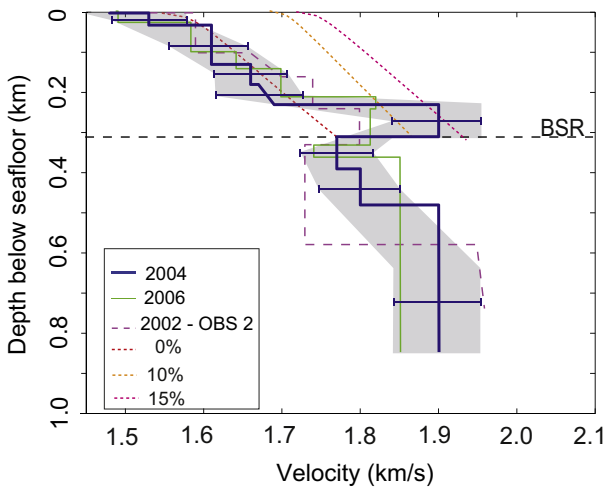

Figure 9. 1-D velocity-depth profile (thick blue line) obtained by averaging the 2004 2-D velocity model at constant depth below the seafloor, with approximate error estimates (grey shaded area) and error bars for the interval velocities based on the sensitivity analysis (Fig. 8). The high-velocity region is more prominent for the 2004 model than for the 2006 model (thin green line) or for the model of LeBlanc et al. (2007) based on a 2002 OBS survey (purple dashed line); OBS 2 from this survey was located 2 km south of the 2004 array. The velocity drop of ~300 m/s at a depth of ~310 m below seafloor indicates the base of the gas hydrate stability zone (GHSZ). The red dashed line is the reference velocity profile calculated with the parameters of Table 1 (Mosher, 2008) and standard rock-physics modelling (Dvorkin et al., 1999; Helgerud et al., 1999) assuming no gas hydrate and free gas in the pore space of the sediments. The orange dashed line is a reference velocity profile with the same physical parameters including 10% gas hydrate in the sediment. However, results of the 2004 model suggest even higher values, about 13 ± 5% (pink dashed line). (For interpretation of the references to colour in this figure legend, the reader is referred to the web version of this article.)

Please cite this article in press as: Schlesinger, A., et al., Seismic velocities on the Nova Scotian margin to estimate gas hydrate and free gas concentrations, Marine and Petroleum Geology (2012), doi:10.1016/j.marpetgeo.2012.03.008

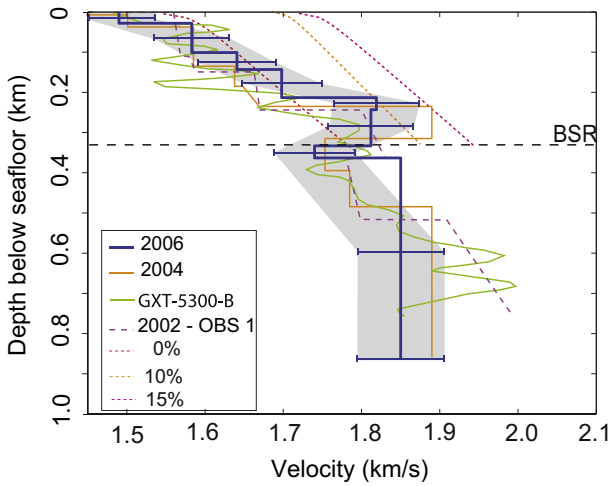

Figure 10. 1-D vertical velocity-depth profile obtained by averaging the 2006 2-D velocity model at constant depth below the seafloor (thick blue line) with approximate error estimates (grey shaded area) and error bars for the interval velocities are shown. The profile is compared with the vertical velocity-depth profile of OBS 1 from the 2002 survey (purple dashed line, LeBlanc et al., 2007) and one vertical velocity-depth profile of Delescluse et al. (2011) that is close to the middle section of the 2006 OBS array (thin green line). Velocities from the region above the recognized BSR are within the 10% bound (orange dashed line) of gas hydrate in the sediment. The velocity contrasts of the 2002 and 2006 model are similar to those achieved by Delescluse et al. (2011); however, the contrasts are smaller than those achieved with the 2004 data (Fig. 9). The red dashed line is the reference velocity profile calculated with the parameters of Table 1 and standard rock-physics modelling (Dvorkin et al., 1999; Helgerud et al., 1999) assuming no gas hydrate and free gas in the sediments. (For interpretation of the references to colour in this figure legend, the reader is referred to the web version of this article.)

occur (reflection 5 – 2004, reflection 6 – 2006, Fig. 3). Although this reflection occurred on all the OBS instruments, it was only picked over a limited offset range of 1–1.5 km from the OBS position, since we followed a conservative picking approach to reduce the picked time-error.

The almost non-reflective nature of the area of the high-velocity region, between the top reflection and the BSR (reflection 6 – 2004, reflection 7 – 2006, Fig. 3), could indicate that gas hydrate cements the sediments and makes them more uniform, as suggested by Katzman et al. (1994) on the Blake Ridge. However, our amplitude decrease above the BSR (Fig. 2) is not as strong as on the Blake Ridge, where there is probably a higher degree of gas hydrate cementation. Large mass-transport deposits were also identified in areas adjacent to the study locations (Campbell et al., 2010) and can possibly be linked to the lower reflectivity of these sediment packages.

6.2. Velocity features: high- and low-velocity layers

A prominent feature in the final 2-D models for the 2004 and 2006 surveys is a high-velocity layer in which the velocity increases by 200–300 m/s (Figs. 9 and 10). With a thickness of approximately 90–110 m, the top of the layer occurs at 220 mbsf, and the base at 310–330 mbsf. Beneath this layer, the velocity decreases by 130 m/s in the 2004 model, but only by 80 m/s in the 2006 model. The velocity decrease occurs at the interface identified as the BSR on 2-D seismic reflection sections (Fig. 2). Thus, we interpret the high-velocity layer as a region of increased gas hydrate concentration. The low-velocity layer beneath the inferred hydrate zone is interpreted to correspond to a zone in which free gas is present.

To compare the final 2-D model results from the 2004 and 2006 data with the results from LeBlanc et al. (2007) and Delescluse et al. (2011), velocities for each interface were averaged with a constant spatial sampling of 100 m across the 2-D velocity profiles (Figs. 9 and 10). Error estimates on the velocities obtained from the sensitivity analysis (Fig. 8) are shown with error bars for each layer. The grey shaded area represents the confidence intervals for the velocities determined by the sensitivity analysis. The averaged 1-D velocity profiles (2004 and 2006) are comparable to results from two OBS stations (OBSs 1 and 2) from the 2002 data of LeBlanc et al. (2007), although there are some distinct differences.

The velocity model of OBS 2 (2002) (Fig. 9 – purple line), which is closest (2 km to the south) to the 2004 OBS array, shows an increase in P-wave velocity of 70 m/s at 230 mbsf. This velocity increase is significantly lower than the one modelled with the 2004 data (300 m/s) for the high-velocity zone above the BSR. However, the 100 m thickness of this high-velocity zone is comparable to the thickness modelled with the 2004 data. Below the BSR, a velocity decrease was modelled with both datasets (2002 and 2004). However, the thickness and velocity values for this layer are significantly different in the two models. The P-wave velocity decreases to 1730 m/s in the 2002 model and the thickness of this layer is about 260 m (LeBlanc et al., 2007). The layer thickness modelled with the 2004 data is only approximately 100 m, and the velocity drop is larger (~130 m/s) than for the 2002 data (~75 m/s).

The velocities modelled for OBS 1 of the 2002 data (Fig. 10 – purple dashed line), which is closest to the 2006 OBS array (1 km north of OBSs 3 and 4), show similar results to OBS 2 of the 2002 survey. The velocity increases by an average of 150 m/s at a depth of 230 mbsf, but drops only by 50 m/s at approximately 360 mbsf. This is comparable to the final model of the 2006 OBSs, where the velocity increases by 130 m/s and decreases by only 50–80 m/s below the high-velocity layer. Hence, the thickness of the high-velocity zone is approximately 120 m for the 2002 data and 2006 data. However, the thickness of the low-velocity zone is much greater for the 2002 OBS 1 (150 m) than for the 2006 data (30 m).

The vertical velocity profile GXT-5300-B (Fig. 10 – green line), which is located approximately in the middle of the 2006 OBS array, was obtained from Delescluse et al. (2011) and is generally consistent with the velocity profile of the 2006 OBS survey. The velocity increases by an average of 130 m/s at 230 mbsf, and drops by only ~70 m/s at a depth of 350 mbsf.

Overall, the velocity contrasts for the 2002 models, for the inferred gas hydrate (high-velocity zone) and free gas layers (low-velocity zone), are closer to the results achieved with the 2006 data and smaller than the velocity contrasts from the 2004 data.

6.3. Gas hydrate concentrations

6.3.1. Calculations and errors

To convert the P-wave velocity to hydrate concentration, the simplest methods basically use just the porosity at a given depth, and require an empirical estimate of the velocity for non-hydrate-bearing sediments (e.g. Lee et al., 1993; Hyndman et al., 1993; Jarrard et al., 1995). The resulting concentrations are directly dependent on the no-hydrate velocity for which the uncertainty is difficult to evaluate.

For the velocity models presented in this study, we used the effective medium theory of Helgerud et al. (1999) to calculate the P-

Table 1
Sediment parameters for the Nova Scotian margin environment modified from Mosher, 2008.

Porosity at seafloor (%)	60
Compaction factor lambda (m)	1000
Composition of Quartz (%), Clay (%)	15, 85

Please cite this article in press as: Schlesinger, A., et al., Seismic velocities on the Nova Scotian margin to estimate gas hydrate and free gas concentrations, Marine and Petroleum Geology (2012), doi:10.1016/j.marpetgeo.2012.03.008

wave velocity for a given gas hydrate concentration. Chand et al. (2004) evaluated a number of different effective medium theories, in which they calculated sediment physical properties from estimates of the porosity, clay-content and quartz-content. The models predicted similar variations of P-wave velocity with hydrate concentration, but the most consistent values for the no-hydrate velocity were found using the theories of Helgerud et al. (1999) and Jakobsen et al. (2000). The calculations were validated by comparisons with velocities determined from drill holes using independent methods. The geological environments tested included both sand-rich sediments (Mackenzie Delta) and clay-rich sediments (Blake Ridge, where sediment compositions are similar to those on the Nova Scotia margin). In our calculations on the Scotia margin, the sediment parameters were taken from LeBlanc et al. (2007) (Table 1). Using effective medium theory, we calculated a reference velocity profile corresponding to no gas hydrate or free gas in the pore space (Figs. 9 and 10 – fine red dashed line), plus two other profiles in which the bulk gas hydrate concentration is 10% and 15% (Figs. 9 and 10).

The calculated gas hydrate concentrations for the 2006 modelled velocities are approximately 2–11% of the pore space. These values are slightly larger than the 2–6% concentrations of bulk gas hydrate estimated from the nearby OBS 1 in the study of LeBlanc et al. (2007). However, the modelled velocities for the 2004 data are higher, corresponding to a greater gas hydrate concentration of approximately 8–18% in the pore space. This is our best estimate of the concentration range for the 2004 data, corresponding to an approximate velocity uncertainty of ±75 m/s; however, a larger range cannot be excluded since our sensitivity analysis provides only a rough velocity uncertainty of ±50–100 m/s.

The reference profile for no gas hydrate is not explicitly included in the error estimate above, which deals with just velocity uncertainties. The concentration is also dependent on specific physical parameters of the sediments, such as the seafloor porosity and the compaction factor, which defines the rate of the depth-dependent porosity decrease (Table 1). For example, if the seafloor porosity is decreased by 3%, the calculated reference velocity profile for no gas hydrate increases by ~50 m/s, so it is near the upper bound of our confidence limit for the no-hydrate region above 220 mbsf. Hence, the calculated gas hydrate concentrations would show a decrease of 2% compared to the ranges calculated above. In contrast, increasing the seafloor porosity by 3% decreases the average reference velocities by 30 m/s, but the calculated values for gas hydrate concentration increase by ~10%. Therefore, we feel that our selected seafloor porosity of 60%, based on LeBlanc et al. (2007), represents a conservative estimate for gas hydrate concentrations.

6.3.2. Lateral variation in hydrate concentration

The OBS sites of this study are located near the eastern sidewall of the Mohican Channel (Fig. 1). The 2004 OBS array, oriented north to south, is parallel and very close to the channel wall, whereas the 2006 OBS array is oriented west to east, perpendicular to the channel wall and extending away from it. In the final 2-D velocity models, velocity values and calculated gas hydrate concentrations for the layer above the BSR are significantly higher for the 2004 data than for the 2006 data. That is, gas hydrate concentrations generally appear to decrease with distance from the Mohican Channel. This pattern is consistent with the 2–6% gas hydrate concentrations derived for the 2002 data for OBS 1, located east of the channel (LeBlanc et al., 2007). Here, the decreasing gas hydrate concentrations with increasing distance from the channel is explained as an effect of lower porosity within the mud-dominant sediment at the depth of the BSR.

A similar pattern was observed in the 2-D reflection seismic datasets, for which BSRs occur in patches distributed over the Scotian margin, and are mainly located where channel structures appear (Cullen et al., 2008; Mosher, 2011). Although most of the Scotian margin sediments are fine-grained, glacially-derived, marine sediments with a high percentage of clay (Mosher, 2008), coarser grained deposits were probably transported in the outwash channels (e.g. Mohican Channel) and deposited over the sidewalls and foot of the channel.

Mosher (2011) stated that most of the recognized BSRs are within large sedimentary drift deposits that were transported during the Miocene and Pliocene (Campbell et al., 2010). Recent studies show that the Pleistocene-to-recent Mohican Channel cuts through these deposits, exhibiting various episodes of cut-and-fill during this period (Campbell et al., 2010; Mosher, 2011). The occurrence of gas hydrate is likely linked to grain-sorting and porosity changes that establish potential reservoir rocks along the Mohican Channel.

Recent studies from the Svalbard margin by Chabert et al. (2011) show similar results, where the formation of gas hydrate is controlled by lithology, which varies downslope from glacial-marine sediments to finer hemipelagic sediments. According to Chabert et al. (2011), gas hydrate concentrations in glacial-marine sediments are too small to produce a prominent increase in P-wave velocity. Estimated gas hydrate concentrations within the sediment frame, modelled using effective medium modelling (Helgerud et al., 1999) amongst others, range between 5% and 12% (Chabert et al., 2011). Another study from the mid-Norwegian margin by Bünz et al. (2005) shows a discontinuous BSR along the margin at the Storegga slide. Gas hydrate estimates are within a range of 3–6% of the pore space assuming hydrate as a component of the sediment frame using effective medium modelling (Bünz et al., 2005).

A key feature of the gas hydrate distribution on the passive Scotian margin, based on the seismic velocity analyses, is that the hydrate is distributed in the ~100 m thick region just above the BSR, with no indications of gas hydrate occurring between the seafloor and the top of that layer (~220 mbsf). Malinverno et al. (2008) presented modelling results from the Cascadia margin to show that this could be produced, either by low sedimentation rates or by low rates of diffusive upward fluid flow. On the passive Scotian margin, the low fluid flux rates are likely the dominant factor in restricting gas hydrate to the layer above the BSR.

6.4. Free gas concentrations

Laboratory studies (e.g. Lee, 2004) show that very small concentrations of free gas in the pore space can have a large velocity effect. Concentrations as small as 1% can reduce the P-wave velocity by more than 5%, or approximately 90 m/s (LeBlanc et al., 2007). Those free gas concentrations were calculated based on the rock-physics models presented by Helgerud et al. (1999) and Dvorkin et al. (1999). Similar velocity decreases of 50–80 m/s, as modelled with the 2006 dataset, and 130 m/s, modelled with the 2004 dataset, correspond to concentrations of 1–2% gas in the sediments at depths of 310–330 mbsf. The modelled thickness for this low-velocity layer beneath the BSR is approximately 30–150 m.

Our results for gas zone thickness are consistent with Xu and Ruppel (1999) and Haacke et al. (2008), who argue that a thick free gas zone is associated with passive margins with low rates of methane flux (<few tenths mm/yr, Haacke et al., 2007) and slower seafloor uplift, in contrast to active margins where a thin free gas zone (~10–30 m) is produced with high rates of upward directed fluid flux (>few tenths of mm/yr, Haacke et al., 2007) and high rates of seafloor uplift (e.g., accretionary wedges).

Please cite this article in press as: Schlesinger, A., et al., Seismic velocities on the Nova Scotian margin to estimate gas hydrate and free gas concentrations, Marine and Petroleum Geology (2012), doi:10.1016/j.marpetgeo.2012.03.008

The 1-D vertical velocity profiles obtained by Delescluse et al. (2011) show smaller contrasts between the two velocity zones at the BSR depth with increasing distance from the Mohican Channel. In addition to the velocity profile GXT-5300-B (Fig. 10), Delescluse et al. (2011) modelled another vertical velocity profile that is located several kilometres to the west of the 2006 OBS array, at the edge of the Mohican Channel. The results show a velocity decrease of 200 m/s below the BSR depth. The lower velocity is most likely a result of higher gas concentrations within the sediments that are closer to the Mohican Channel.

6.5. OBS surveys

As the final velocity models of both surveys (2004 and 2006) show, the geometry for OBS surveys is crucial to the obtained results. Choosing the appropriate instrument spacing (<500 m) is essential for modelling the velocity contrasts produced by even small amounts of gas hydrate in the pore space of shallow sediments. Large shot offsets (>5 km) to both sides of the instruments are also necessary to detect refracted and wide-angle reflected arrivals from below the BSR that constrain the velocities in these deep regions.

7. Conclusions

The velocity structure beneath the Scotian margin off eastern Canada was modelled in a travel-time inversion approach using ocean-bottom seismometer and single-channel seismic data. Careful analysis and modelling permitted the small velocity anomalies associated with low concentrations of gas hydrate and free gas to be resolved. A high-velocity zone, occurring over the depth range of ~220–330 mbsf with a modelled velocity increase of 200–300 m/s, is interpreted as a gas hydrate layer. Depending on the chosen rock-physics model and a depth-dependent no gas hydrate background velocity model, the modelled velocity increase implies gas hydrate concentrations of 4–13% of the pore space. The presumed gas hydrate is located just above the identified bottom-simulating reflection. The region between the seafloor and the top of the gas hydrate layer (~220 mbsf) shows no indications of gas hydrate, which may be explained by the low diffusive fluid flux rates common for passive margins (e.g. Haacke et al., 2007). Based on results from three seismic surveys between 2002 and 2006, gas hydrate concentrations generally decrease with relative distance from the Mohican channel structure. The decreasing velocity contrast at the BSR depth with relative distance from the Mohican Channel, as concluded by Delescluse et al. (2011), strengthens this argument.

Beneath the bottom-simulating reflection, the velocity decreases by approximately 130 m/s, which corresponds to free gas concentrations of 1–2% of the sediment pore space. The thickness of the free gas layer is 30–150 m, which is significantly greater than for most active continental margins (10–30 m). The low concentrations and thicker layer for this passive margin are probably a consequence of the low upward directed fluid flux rates.

Acknowledgements

The authors thank the crew and staff of CCGS Hudson for their dedication in acquiring the seismic data used in this study. The work was supported by grants from the Natural Science and Engineering Research Council to K. Louden, D. Mosher, R. Hyndman and G. Spence, and from the Climate Change Technology and Innovation (CCTI) program to R. Hyndman. Natural Resources Canada, Earth Science Sector, Gas Hydrate: Fuel for the Future program funded the research expeditions to acquire the data used in this study. The Climate Change Technology and Innovation Research and Development Initiative, Natural Resources Canada, partially funded development of the ocean-bottom seismometers (OBS).

Further thanks go to Christan Berndt, Michael Riedel and an anonymous reviewer for their helpful ideas and criticism. Velocity figures and maps were prepared with GMT software (Wessel and Smith, 1995) and seismic data were processed and plotted using the Seismic Unix software.

References

Bünz, S., Mienert, J., Vanneste, M., Andreassen, K., 2005. Case Study. Gas hydrates at the Storegga Slide: constraints from an analysis of multicomponent, wide-angle seismic data. Geophysics 70 (5), B19–B34.

Campbell, C.D., Mosher, D.C., Shimeld, J.W., 2010. Erosional unconformities, mega-slumps and giant mud waves: insights into passive margin evolution from the continental slope off Nova Scotia. In: Central and North American Conjugate Margins Conference: Re-discovering the Atlantic, New Winds from an Old Sea, Lisbon 2010, vol. IV, pp. 37–41.

Chabert, A., Minshull, T.A., Westbrook, G.K., Berndt, C., Thatcher, K.E., Sarkar, S., 2011. Characterization of a stratigraphically constrained gas hydrate system along the western continental margin of Svalbard from ocean bottom seismometer data. Journal of Geophysical Research 116, 16.

Chand, S., Minshull, T.A., Gei, D., Carcione, J.M., 2004. Elastic velocity models for gas-hydrate-bearing sediments–a comparison. Geophysical Journal International 159 (2), 573–590.

Cullen, J., Mosher, D.C., Louden, K.E., 2008. The Mohican channel gas hydrate zone, Scotian Slope, Geophysical structure. In: Proceedings of the 6th International Conference on Gas Hydrates (ICGH2008).

Dai, J., Xu, H., Snyder, F., Dutta, N., 2004. Detection and estimation of gas hydrates using rock physics and seismic inversion: examples from the northern deepwater Gulf of Mexico. The Leading Edge 23 (1), 60–66.

Delescluse, M., Nedimovic, M.R., Louden, K.E., 2011. Case History – 2D waveform tomography applied to long-streamer MCS data from the Scotian Slope. Geophysics 76 (4), B151–B163.

Dvorkin, J., Prasad, M., Sakai, A., Lavoie, D., 1999. Elasticity of marine sediments: rock physics modelling. Geophysical Research Letters 26 (12), 1781–1784.

Haacke, R.R., Westbrook, G., Hyndman, R., 2007. Gas hydrate, fluid flow and free gas: formation of the bottom-simulating reflector. Earth and Planetary Science Letters 261, 407–420, 17 pp.

Haacke, R.R., Westbrook, G., Riley, M., 2008. Controls on the formation and stability of gas hydrate related bottom-simulating reflectors (BSRs): a case study from the west Svalbard continental slope. Journal of Geophysical Research 113.

Helgerud, M.B., Dvorkin, J., Nur, A., Sakai, A., Collett, T., 1999. Elastic-wave velocity in marine sediments with gas hydrates: effective medium modelling. Geophysical Research Letters 26 (13), 2021–2024.

Holbrook, W.S., Hoskins, H., Wood, W.T., Stephen, R.A., Lizarrade, D., 1996. Methane hydrate, bottom-simulating reflectors, and gas bubbles: results of vertical seismic profiles on the Blake Ridge. Science 273, 1840–1843.

Hyndman, R.D., Moore, G.F., Moran, K., 1993. Velocity, porosity, and pore-fluid loss from the Nankai subduction zone accretionary prism. In: Hill, I.A., Taira, A., Firth, J.V., et al. (Eds.), 1993. Proceedings of the Ocean Drilling Program, Scientific Results, vol. 131, College Station, TX, pp. 211–220.

Jakobsen, M., Hudson, J.A., Minshull, T.A., Singh, S.C., 2000. Elastic properties of hydrate-bearing sediments using effective medium theory. Journal of Geophysical Research 105, 561–577.

Jaiswal, P., Zelt, C.A., Pecher, I.A., 2006. Seismic characterization of a gas hydrate system in the Gulf of Mexico using wide-aperture data. Geophysical Journal International 165, 108–120.

Jarrard, R.D., MacKay, M.E., Westbrook, G.K., Screaton, E.J., 1995. Log-based porosity of ODP sites on the Cascadia accretionary prism. In: Carson, B., Westbrook, G.K., Musgrave, R.J., Suess, E. (Eds.), Proceedings of the Ocean Drilling Program, Scientific Results, 146 (Part 1), College Station, TX, pp. 313–335.

Katzman, R., Holbrook, W.S., Paull, C.K., 1994. Combined vertical-incidence and wide-angle seismic study of a gas hydrate zone, Blake Ridge. Journal of Geophysical Research 99, 17,975–17,995.

LeBlanc, C., Louden, K., Mosher, D., 2007. Gas hydrates off Eastern Canada: velocity models from wide-angle seismic profiles on the Scotian Slope. Marine and Petroleum Geology 24, 321–335.

Lee, M.W., Hutchinson, D.R., Dillon, W.P., Miller, J.J., Agena, W.F., Swift, B.A., 1993. Method of estimating the amount of in-situ gas hydrates in deep marine sediments. Marine and Petroleum Geology 10 (5), 493–506.

Lee, M.W., 2004. Elastic velocities of partially gas-saturated unconsolidated sediments. Marine and Petroleum Geology 21, 641–650.

Lopez, C., Spence, G., Hyndman, R., Kelley, D., 2010. Frontal ridge slope failure at the northern Cascadia margin: margin-normal fault and gas hydrate control. Geology 38 (11). doi:10.1130/G31136.1.

Please cite this article in press as: Schlesinger, A., et al., Seismic velocities on the Nova Scotian margin to estimate gas hydrate and free gas concentrations, Marine and Petroleum Geology (2012), doi:10.1016/j.marpetgeo.2012.03.008

Malinverno, A., Kastner, M., Torres, M.E., Wortmann, U.E., 2008. Gas hydrate occurrence from pore water chlorinity and downhole logs in transect across the northern Cascadia margin (Integrated Ocean Drilling Program Expedition). Journal of Geophysical Research 1 (13), B08103.

Mosher, D.C., Piper, D.J., Campbell, D.C., Jenner, K.A., 2004. Near surface geology and sediment-failure geohazards of the central Scotian Slope. AAPG 88, 703–723.

Mosher, D., 2004. Hudson 2004-030 Cruise Report: July 10–20, 2004. Geological Survey of Canada (Atlantic), Open File, 72 p.

Mosher, D., 2008. Bottom simulating reflectors on Canada's east coast margin: evidence for gas hydrate. In: Proceedings of the 6th International Conference on Gas Hydrates (ICGH 2008).

Mosher, D., 2011. A margin-wide BSR gas hydrate assessment: Canada's Atlantic margin. Marine and Petroleum Geology 28 (8), 1540–1553.

Neave, K.G., 1990. Shallow seismic velocities on the eastern Grand Banks and Flemish Pass. Unpublished report Prepared for Alan Judge of the Terrain Sciences Division, Geological Survey of Canada, 19 p.

Ruppel, C., Collett, T., Boswell, R., Lorenson, T., Buczkowski, B., Waite, W., 2011. A new global gas hydrate drilling map based on reservoir type. Fire in the Ice, DOE NETL Newsletter 11 (1), 13–17.

Tucholke, B.E., Bryan, G.M., Ewing, J.I., 1977. Gas hydrate horizons detected in seismic-profiler data from the western North Atlantic. American Association of Petroleum Geologists Bulletin 61, 689–707.

Wessel, P, Smith, W.H.F., 1995. New version of the Generic Mapping Tool released. Eos, Transactions of the American Geophysical Union 76 (33), 329.

Xu, W., Ruppel, C., 1999. Predicting the occurrence, distribution, and evolution of methane gas hydrate in porous marine sediments from analytical models. Journal of Geophysical Research 104, 5081–5096.

Zelt, C.A., Smith, R.B., 1992. Seismic travel-time inversion for 2-D crustal velocity structure. Geophysical Journal International 108, 16–34.

Zykov, M., 2006. 3-D travel time tomography of the gas hydrate area offshore Vancouver Island based on OBS data. PhD Thesis with the University of Victoria, BC, Canada.

Please cite this article in press as: Schlesinger, A., et al., Seismic velocities on the Nova Scotian margin to estimate gas hydrate and free gas concentrations, Marine and Petroleum Geology (2012), doi:10.1016/j.marpetgeo.2012.03.008